This is a repository copy of *openBF: an open-source finite volume 1D blood flow solver*.

PAPER • OPEN ACCESS

openBF: an open-source finite volume 1D blood flow solver

View the article online for updates and enhancements.

Physiological Measurement

IPEM
Institute of Physics and
Engineering in Medicine

CrossMark

PAPER

openBF: an open-source finite volume 1D blood flow solver

I Benemerito[1,2,*] ⓘ, A Melis[3] ⓘ, A Wehenkel[4] ⓘ and A Marzo[1,2] ⓘ

[1] INSIGNEO Institute for *in-silico* medicine, University of Sheffield, Sheffield, United Kingdom
[2] Department of Mechanical Engineering, University of Sheffield, Sheffield, United Kingdom
[3] VivaCity, London, United Kingdom
[4] University of Liege, Liege, Belgium
[*] Author to whom any correspondence should be addressed.

E-mail: i.benemerito@sheffield.ac.uk

Abstract

Computational simulations are widely adopted in cardiovascular biomechanics because of their capability of producing physiological data otherwise impossible to measure with non-invasive modalities. *Objective.* This study presents openBF, a computational library for simulating the blood dynamics in the cardiovascular system. *Approach.* openBF adopts a one-dimensional viscoelastic representation of the arterial system, and is coupled with zero-dimensional windkessel models at the outlets. Equations are solved by means of the finite-volume method and the code is written in Julia. We assess its predictions by performing a multiscale validation study on several domains available from the literature. *Main results.* At all scales, which range from individual arteries to a population of virtual subjects, openBF's solution show excellent agreement with the solutions from existing software. For reported simulations, openBF requires low computational times. *Significance.* openBF is easy to install, use, and deploy on multiple platforms and architectures, and gives accurate prediction of blood dynamics in short time-frames. It is actively maintained and available open-source on GitHub, which favours contributions from the biomechanical community.

1. Introduction

Diseases of the cardiovascular system represent the first cause of mortality worldwide, with an increasing number of individuals being affected every year (Townsend *et al* 2022). Ischaemic stroke, heart failure and hypertensive disease rank as the most common pathologies (Amini *et al* 2021).

A thorough investigation of these pathologies is often not possible in *in-vivo* settings because of the invasive nature of the investigation itself and, when not using imaging methodologies, it is typically limited to the measurement of pulse wave velocity to infer quantities such as arterial stiffness, which is related to cardiovascular health (Vasan *et al* 2022). On the other hand, their *in-vitro* replications suffer from the difficulty in realistically replicating physiological and pathological scenarios.

In contrast, *in-silico* simulations allow flexibly simulating complex scenarios that are inaccessible with the methodologies mentioned above. Two main approaches are taken in the field: three-dimensional (3D) simulations or reduced order models. 3D simulations produce a detailed representation of the velocity field in complex geometries. They are ideally suited for studying specific pathologies where geometric features such as bending or tortuosity significantly affect the fluid flow (Kashyap *et al* 2022), such as vascular aneurysms. Their elevated computational costs, however, limit their applicability to relatively small regions of interest, with only a few large-domain studies existing in the literature (Xiao *et al* 2013, Caddy *et al* 2024, McCullough and Coveney 2024), and make the analysis of large populations of subjects unfeasible.

One-dimensional (1D) and zero-dimensional (0D) models adopt instead a reduced representation of the system geometry and a simplified description of the underlying physics. The inevitable loss in accuracy, which several studies have quantified as low (Alastruey *et al* 2011, Blanco *et al* 2018, Bertaglia *et al* 2020), is compensated by the flexibility to run extensive population studies and investigate parameters variability with low computational overhead. Several reduced-order models and associated solvers have been proposed in the

Table 1. Open-source 1D blood flow solvers sorted by initial release date. Solvers differ for the programming language, open-source licensing, and the underlying numerical solution method: finite difference (FD), finite element (FE), finite volume (FV), and method of characteristics (MoC).

Solver	Type	Language	License	Last Update
STARFiSh (Hellevik *et al* 2013)	FD	Python	GNU LGPL	2016
Nektar++ (Cantwell *et al* 2015)	FE	C++	MIT	2024
openBF (Melis 2017)	FV	Julia	Apache–2.0	2024
SimVascular (Updegrove *et al* 2017)	FE	C++	BSD	2024
VaMpy (Diem and Bressloff 2017)	FD	Python	BSD3–Clause	2018
CardioFAN (Seyed Vahedein and Liberson 2019)	FV	Matlab	MIT	2019
First_blood (Wéber *et al* 2023)	MoC	C++	MIT	2024

literature (Formaggia *et al* 2001, Sherwin *et al* 2003, Reymond *et al* 2009, Müller and Toro 2014) differing in the numerical scheme employed for the solution of the equations, the assumption of steady vs unsteady flow, or the choice of the constitute equation. However, as shown in table 1, only a few of such models are available open-source, which limits the widespread adoption of this modelling approach within the biomechanical community.

In 2017 we released the first version of openBF (Melis 2017, 2018), the first finite-volume open-source solver specifically aimed at 1D blood flow simulations available to the public domain. By not focusing on developing a general-purpose simulation framework, the code base was designed to be highly modular and optimised to reduce simulation times. Its open-source license allowed for use in multiple scenarios. Being developed in the Julia programming language (Bezanson *et al* 2017) and distributed as a Julia package, it allowed easy setup of simulations and quick implementation of new and experimental features. As a result, openBF was successfully deployed on different architectures, scaling from single CPU to whole HPC clusters, and adopted for the study of cerebral vasospasm (Melis *et al* 2019), ischaemic stroke (Mustafa 2021, Benemerito *et al* 2022, 2023), for creating atlases of the human head (Moura *et al* 2021, Lahtinen *et al* 2023), for modelling of kidney pathologies (Wang *et al* 2024), and in developing simulation-based inference methods for complex cardiovascular systems (Wehenkel *et al* 2023).

In this paper, an updated and validated version of openBF is presented. Formerly based on a purely-elastic mathematical model, we introduce a new viscoelastic solver and an accompanying web-based GUI (https://openbf.streamlit.app) providing tools for arterial network creation and results analysis. The solver code and its documentation are available through a GitHub repository at https://github.com/INSIGNEO/openBF, and with an associated DOI at https://zenodo.org/records/13850604.

The paper is structured as follows. In section 2, we briefly introduce the mathematical model and the numerical scheme adopted for its solution. Section 3 presents the case studies for the multi-scale validation of the solver: we test openBF against 3D solutions on **a.** single vessels, **b.** human circulatory arterial network, and **c.** on a large population of healthy ageing individuals. Finally, section 4 presents and discusses the simulations results, both in terms of predicted waveforms and computational performances.

2. Mathematical model

In openBF, arteries are modelled as long, narrow, straight and circular vessels with thin, radially compliant viscoelastic walls; blood is assumed to be an incompressible Newtonian fluid. Under these assumptions, the 3D Navier–Stokes equations can be reduced to the 1D system in terms of vessel area A and volumetric flow rate Q (Formaggia *et al* 2010, Melis 2017)

$$\begin{cases} \dfrac{\partial A}{\partial t} + \dfrac{\partial Q}{\partial z} = 0, \\ \dfrac{\partial Q}{\partial t} + \dfrac{\partial}{\partial z}\left(\alpha\dfrac{Q^2}{A}\right) + \dfrac{A}{\rho}\dfrac{\partial P}{\partial z} = -2\dfrac{\mu}{\rho}\left(\gamma+2\right)\dfrac{Q}{A}, \\ P(A) = P_{\text{ext}} + \dfrac{\beta}{A_0}\left(\sqrt{A}-\sqrt{A_0}\right) - \dfrac{\Gamma}{A_0\sqrt{A}}\dfrac{\partial Q}{\partial z}, \end{cases} \tag{1}$$

where t is time, z is the vessel longitudinal coordinate, A is the cross-sectional area, A_0 is the vessel reference area, Q is volumetric flow rate, P intramural pressure, P_{ext} is the external pressure, ρ is blood density, μ is blood viscosity, and β and Γ are elastic and viscous coefficients, respectively. The first equation represents the conservation of mass, the second one expresses the conservation of linear momentum and the third is a viscoelastic constitutive law based on Kelvin–Voigt model (Ghigo 2017). A purely elastic cases can be obtained by setting $\Gamma = 0$. Viscous losses can be calibrated by choosing the value of γ, which models the

Figure 1. Example of typical ascending aorta volumetric flow rate as function of time used as inlet boundary condition. The waveform is normalised on the cardiac cycle period T_c.

Figure 2. Schematic of three-element windkessel used as outlet boundary condition.
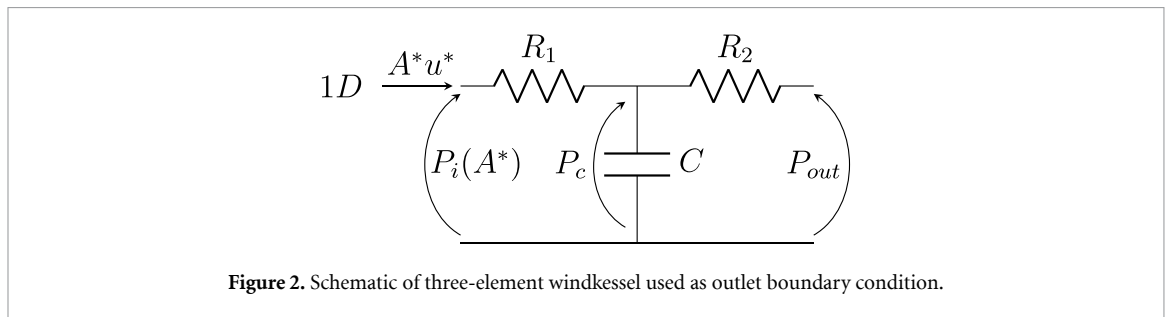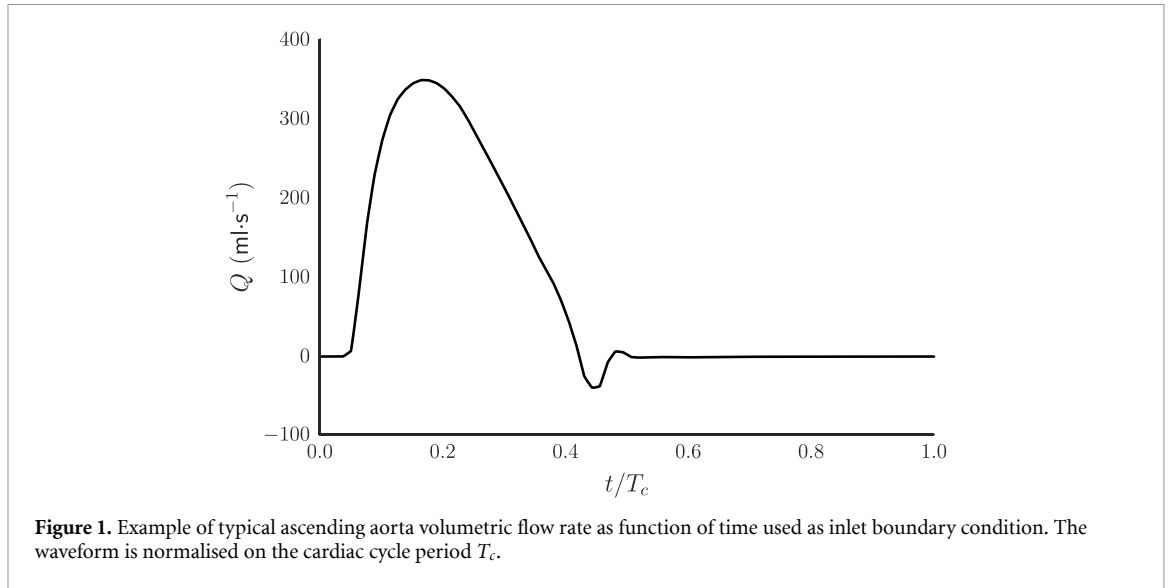
shape of the velocity profile. Multiple vessels are linked together assuming no energy losses at bifurcation sites (Formaggia *et al* 2003, Milišic and Quarteroni 2004).

The numerical solution in terms of A, Q and P is obtained via the second-order MUSCL numerical scheme (van Leer 1979, LeVeque 2002). This is a shock-capturing n-order in time and space (fixed to the second-order in openBF) finite-volume explicit method used for hyperbolic sets of equation. The finite-volume formulation is particularly suited (Wang *et al* 2016) to problems involving abrupt changes in the solution (pressure shock-waves) and discontinuous domain, e.g. bifurcations, local changes in mechanical properties such as stenosis, atherosclerosis and aneurysms, and multi-scale models coupling. Values of time steps are space discretisation of the computational domain are chosen to satisfy the Courant–Friedrichs–Levy stability condition (Courant 1928).

The system 1 is closed by a periodic inflow waveform (figure 1) and terminal outlet boundary conditions via three-element windkessel models coupling (Fernández *et al* 2005, Peiró and Veneziani 2009) (figure 2). The windkessel equation reads

$$\begin{cases} A^* u^* \left(1 + \dfrac{R_1}{R_2} \right) + C R_1 \dfrac{\partial (A^* u^*)}{\partial t} = \dfrac{P_e - P_{\text{out}}}{R_2} + C_c \dfrac{\partial P_i}{\partial t}, \\ C \dfrac{\partial P_c}{\partial t} = A^* u^* - \dfrac{P_c - P_{\text{out}}}{R_2}, \end{cases} \tag{2}$$

where R_1 and R_2 are the proximal and peripheral resistances, C is the peripheral compliance, P_{out} is the outlet pressure (assumed to be zero at capillary level), P_c is the pressure across C and P_i is pressure at the 0D/1D interface. The model is solved iteratively by Newton's method in function of A^* and u^* (area and flow velocity at interface, respectively) which are initialised with values from the intermediate 1D solution.

While the assumptions listed above, for example no energy loss at bifurcations or the use of three-element windkessel as outlet boundary conditions, are hard-wired into the model, the open-source nature of the code gives to users and contributors from the community the possibility to implement more specific modelling assumptions.

Table 2. Network parameters for single vessel simulations: thoracic aorta (TA) and common carotid artery (CCA) (Boileau *et al* 2015).

Parameter	TA	CCA
L [cm]	24.137	12.6
R_0 [mm]	9.87	2.6485
h_0 [mm]	0.82	0.24
E [kPa]	400	700
R_1 [MPa s m^{-3}]	1.1752	2.4875
R_2 [MPa s m^{-3}]	1.1167	1.8697
C_c [m^3 GPa^{-1}]	10.163	0.1753

Table 3. Iliac bifurcation network parameters (Boileau *et al* 2015).

Parameter	Parent	Child 1	Child 2
L [cm]	8.6	8.5	8.5
R_0 [mm]	7.581	5.492	5.492
h_0 [mm]	0.9	0.68	0.68
E [kPa]	500	700	700
R_1 [MPa s m^{-3}]		6.8123	6.8126
R_2 [MPa s m^{-3}]		0.31	0.31
C_c [m^3 GPa^{-1}]		0.366	0.366

3. Multiscale validation

In order to perform a thorough evaluation of openBF's performance we compare its results against a number of benchmark cases that describe the physiology of the cardiovascular system at different spatial scales: we simulate single vessels and bifurcations (section 3.1), the entire arterial systemic circulation (section 3.2) and a population of healthy, ageing individuals (section 3.3). In all cases we run the solver until convergence of all pressure waveforms across an entire cardiac cycle, i.e. the pressure waveform root mean square errors between two consecutive cardiac cycles is less than 1%.

3.1. Single arteries and iliac bifurcation

We benchmark openBF against 1D and 3D reference solutions on the case of single, reflection free arteries (upper thoracic aorta, common carotid artery) and in the case of the iliac bifurcation (Boileau *et al* 2015). Geometrical and structural parameters for single arteries and for the bifurcation are reported in tables 2 and 3, respectively. To allow for a proper comparison with benchmark data, we used the elastic tube law ($\Gamma = 0$) for this set of simulations.

3.2. Systemic circulation

We use the ADAN56 model (Blanco *et al* 2014) as benchmark for the systematic circulation. The model consists of 61 segments from 56 major arteries, coupled to 31 windkessel model as outlets. The inlet flow-rate is applied at the ascending aorta. Geometrical and structural parameters are not provided here because this is a very well established model, and we refer the reader to the original publication for further details (Blanco *et al* 2014). Since openBF does not account for vessel tapering, in case of tapered vessels we used the mean of the proximal and distal radii rather than using two different values.

3.3. Healthy ageing population

Ageing is considered amongst the most important risk factor for cardiovascular pathologies. A number of researchers have developed ageing models of the cardiovascular system (Guala *et al* 2017, Pagoulatou and Stergiopulos 2017), incorporating within them changes in radii, stiffness and cardiac performances. Charlton and colleagues (Charlton *et al* 2019) have developed and made publicly available a dataset of pressure, area and velocity waveforms from fifteen arteries of 4374 virtual, healthy ageing individuals. We used this dataset to produce matching openBF's models, and evaluate them on the following metrics: diastolic and systolic brachial pressure, systolic aortic pressure, pulse pressure in brachial and ascending aorta, pulse pressure amplification, and augmentation pressure.

In addition to using these aggregated values, we assess openBF's solution on eleven arteries by computing the errors presented in section 3.4.

3.4. Error calculation

We use a number of well-established metrics to analytically quantify the difference between openBF's solution and the literature ones for the single arteries, bifurcation and systemic circulation cases. As proposed by Wang *et al* (2016) and others (Boileau *et al* 2015), we use the following relative error metrics for *P* and *Q*:

$$\mathcal{E}_P^{\text{RMS}} = \sqrt{\frac{1}{n}\sum_{i=1}^{n}\left(\frac{P_i^{\text{oBF}} - \mathcal{P}_i}{\mathcal{P}_i}\right)^2}, \qquad \mathcal{E}_Q^{\text{RMS}} = \sqrt{\frac{1}{n}\sum_{i=1}^{n}\left(\frac{Q_i^{\text{oBF}} - \mathcal{Q}_i}{\mathcal{Q}_i}\right)^2}, \qquad (3)$$

$$\mathcal{E}_P^{\text{MAX}} = \max_i \left|\frac{P_i^{\text{oBF}} - \mathcal{P}_i}{\mathcal{P}_i}\right|, \qquad \mathcal{E}_Q^{\text{MAX}} = \max_i \left|\frac{Q_i^{\text{oBF}} - \mathcal{Q}_i}{\max_i \mathcal{Q}_i}\right|, \qquad (4)$$

$$\mathcal{E}_P^{\text{SYS}} = \frac{\max P^{\text{oBF}} - \max \mathcal{P}}{\max \mathcal{P}}, \qquad \mathcal{E}_Q^{\text{SYS}} = \frac{\max Q^{\text{oBF}} - \max \mathcal{Q}}{\max \mathcal{Q}}, \qquad (5)$$

$$\mathcal{E}_P^{\text{DIAS}} = \frac{\min P^{\text{oBF}} - \min \mathcal{P}}{\min \mathcal{P}}, \qquad \mathcal{E}_Q^{\text{DIAS}} = \frac{\min Q^{\text{oBF}} - \min \mathcal{Q}}{\max \mathcal{Q}}, \qquad (6)$$

where P_i^{oBF} and Q_i^{oBF} indicate the openBF's solution in pressure and flow-rate respectively, at the *i*th time point during the cardiac cycle. Likewise, with $\mathcal{P}_i$ and $\mathcal{Q}_i$ we indicate the reference pressure and flow-rate solutions from the literature. $\mathcal{E}_P^{\text{RMS}}$ and $\mathcal{E}_Q^{\text{RMS}}$ are the root mean square relative errors for pressure and flow-rate. Maximum relative errors in pressure and flow are $\mathcal{E}_P^{\text{MAX}}$ and $\mathcal{E}_Q^{\text{MAX}}$, while errors at systole and diastole are identified by apices SYS and DIAS.

To validate the results at the population scale, we assess openBF's predictions on a number of ageing related pressure measurements (diastolic and systolic pressure in ascending aorta and brachial artery, pulse pressure in ascending aorta and brachial artery, pulse pressure amplification and augmentation pressure in the brachial artery). These quantities are chosen because they are reported in Charlton *et al* (2019).

To quantify the shape similarity of openBF's waveforms with the reference dataset we adopt dynamic time warping (DTW) (Müller 2007), implemented through the Python library DTAIDistance (Meert 2020). Given two time series, DTW computes the similarity of two time series by defining a cost matrix associated with the number of steps required for deforming one series into the other. This number of steps is referred to as the distance *d*. At the same time, the DTW algorithm provides the optimal (lowest cost) warping path, whose length we will denote as *L*. We use the following as error metric:
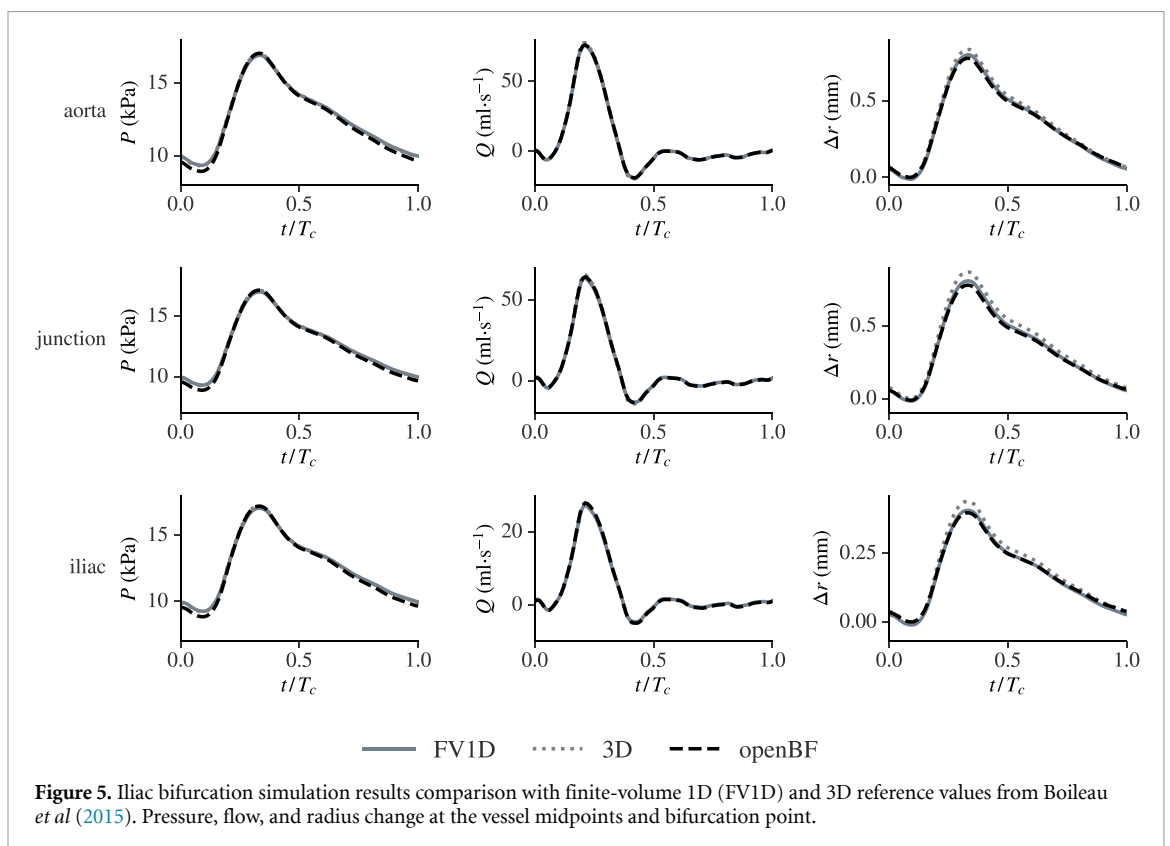
$$\mathcal{E}_v^{\text{DTW}} = \frac{d}{L}, \qquad (7)$$

where *v* denotes either pressure, area or velocity. In this study we compute the normalised distance $\mathcal{E}_v^{\text{DTW}}$ between openBF and Charlton's solution for eleven arteries of all patients. The eleven arteries are those reported in Charlton *et al* (2019).

4. Results and discussion

4.1. Single arteries and iliac bifurcation

Pressure and flow-rate waveforms measured at the vessels' midpoint for the benchmark cases are reported in figures 3–5. The figure also reports changes in arterial radius and inlet-outlet pressure difference during the cardiac cycle. It can be observed that the agreement between openBF and the reference solutions is excellent for all the variables considered (table 4). In particular, errors are within 7% w.r.t. the 1D solution. openBF's solution is also in agreement with 3D simulations as the main flow features are captured but the maximum ΔP is underestimated of 35% in the upper thoracic aorta. This is ascribable to the mathematical founding assumptions on small radial displacements and straight geometry, two major simplifications about the aorta topology. Eventually, the bifurcation 1D waveforms match the 3D simulation with errors $\leqslant 10\%$. This final result indicates that openBF is capable of accurately simulating wave reflections at junction and peripheral sites, an important feature needed to simulate more complex networks.

Figure 3. Upper thoracic aorta single vessel simulation results comparison with finite-volume 1D (FV1D) and 3D reference values from Boileau *et al* (2015). Pressure, flow and radius change at the midpoint of the vessel, and pressure difference between outlet and inlet.

Figure 4. Common carotid artery single vessel simulation results comparison with finite-volume 1D (FV1D) and 3D reference values from Boileau *et al* (2015). Pressure, flow and radius change at the midpoint of the vessel, and pressure difference between outlet and inlet.

Figure 5. Iliac bifurcation simulation results comparison with finite-volume 1D (FV1D) and 3D reference values from Boileau *et al* (2015). Pressure, flow, and radius change at the vessel midpoints and bifurcation point.

4.2. Systemic circulation

Figure 6 and table 5 show that openBF's solution to the wave propagation and reflection problem on the ADAN56 network is in close agreement with the results from Boileau *et al* (2015), with pressure waveform errors within 8% across the entire arterial tree. Higher differences are observed in the internal carotid artery

Table 4. Upper thoracic aorta (UTA), common carotid artery (CCA), and iliac bifurcation simulations percentage relative errors w.r.t. finite-volume 1D (FV1D) and 3D results from Boileau *et al* (2015).

		UTA		CCA		Bifurcation	
		FV1D	3D	FV1D	3D	FV1D	3D
$\mathcal{E}^{\mathrm{RMS}}$	P	0.69	1.83	0.09	0.37	0.31	0.44
	ΔP	0.08	7.94	0.8	5.01		
	Q	0.79	2.96	0.31	0.60	1.08	0.45
	Δr	0.59	3.05	0.36	1.44	4.08	4.20
$\mathcal{E}^{\mathrm{MAX}}$	P	2.83	6.01	0.14	0.80	0.80	0.91
	ΔP	6.42	35.55	4.02	19.62		
	Q	4.18	11.25	0.42	1.49	3.28	1.13
	Δr	4.06	11.26	0.20	2.48	6.95	10.30
$\mathcal{E}^{\mathrm{SYS}}$	P	0.33	−0.38	0.03	−0.26	−0.72	0.04
	ΔP	−2.24	−10.77	−2.13	−16.97		
	Q	0.26	−5.03	0.03	−0.53	−3.26	−0.11
	Δr	−1.25	−4.11	−1.32	−2.32	−6.88	−7.33
$\mathcal{E}^{\mathrm{DIAS}}$	P	0.18	1.17	−0.23	0.05	0.57	−0.15
	ΔP	4.25	10.53	0.60	5.05		
	Q	−0.09	3.31	0.03	0.27	1.74	0.25
	Δr	−0.87	1.18	1.37	1.49	−1.89	−10.00

Table 5. ADAN56 simulation errors w.r.t finite-volume 1D results from Boileau *et al* (2015), largest errors per type are highlighted in bold. Pressure and flow values measured at midpoints of aortic arch (AAI), thoracic aorta (TAIII), abdominal aorta (AAV), right common carotid (CCR), right renal (RR), right common iliac (CIR), internal carotid (ICR), right radial (RRA), right posterior interosseous (PIR), right femoral (FIR) and right anterior tibial artery (ATR).

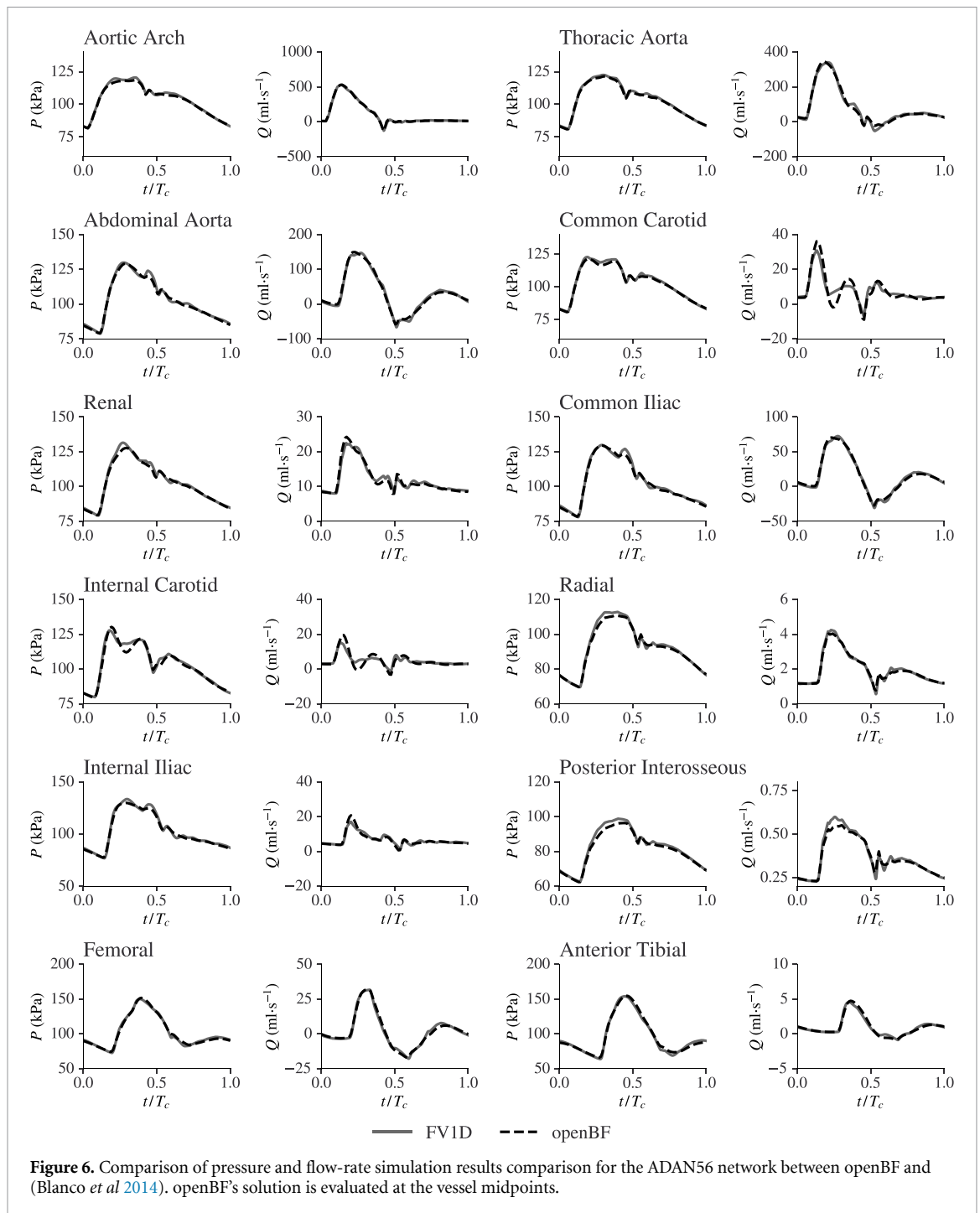|	P				Q			
	$\mathcal{E}^{\mathrm{RMS}}$	$\mathcal{E}^{\mathrm{MAX}}$	$\mathcal{E}^{\mathrm{SYS}}$	$\mathcal{E}^{\mathrm{DIAS}}$	$\mathcal{E}^{\mathrm{RMS}}$	$\mathcal{E}^{\mathrm{MAX}}$	$\mathcal{E}^{\mathrm{SYS}}$	$\mathcal{E}^{\mathrm{DIAS}}$
AAI	1.06	2.33	−1.67	−0.49	2.18	9.37	0.23	−0.99
TAIII	0.99	2.46	−0.91	−0.33	3.77	8.93	1.07	8.85
AAV	1.42	4.13	−0.61	0.21	3.99	9.85	1.53	5.74
CCR	1.08	2.29	−1.07	−0.44	9.49	28.60	17.09	−6.99
RR	1.48	4.03	**−2.89**	0.30	4.27	11.95	7.98	−0.24
CIR	1.52	3.88	−0.22	0.44	3.94	9.92	−2.94	5.04
ICR	1.79	5.23	1.92	−0.62	**12.44**	**39.00**	**28.95**	**−10.93**
RRA	1.42	4.46	−1.89	0.05	2.53	14.46	−4.89	5.17
IIR	1.78	4.07	−2.73	0.90	6.96	22.73	21.74	−4.89
PIR	1.86	3.96	−2.51	−0.35	3.44	14.83	−8.01	−0.42
FRI	1.88	5.25	1.05	2.35	3.76	8.88	0.90	2.19
ATR	**2.71**	**7.80**	0.42	**3.40**	4.56	10.73	3.89	1.55

where the maximum flow-rate error is 39%. In this case, openBF's flow-rate waveform shows oscillatory components during systole of higher intensity than those present in FV1D solution.

4.3. Healthy ageing population

Figure 7 reports the values of the clinical metrics and their trends as a function of the age of the subjects. openBF shows an overall strong agreement on all variables, both in trends and actual values of the clinical metrics. The maximum discrepancy in terms of average diastolic and systolic pressure is smaller than 5 mmHg. However, openBF's standard deviations bands are larger than the reference ones. We also notice that openBF's predictions of pulse pressure amplification and augmentation pressure are consistently lower than reference values.

A detailed DTW analysis of the pressure, velocity and cross-sectional area waveforms shows a good degree of waveform similarity between openBF and Charlton's data: figure 8 shows the heatmaps of their DTW errors, with lower values indicating grater similarity.

Area waveforms show the best shape similarity, with highest errors located in the thoracic aorta $(1.90 \times 10^{-5} \pm 0.41 \times 10^{-5}\,\mathrm{m}^2)$. The distance in ascending aorta, brachial, carotid and common iliac arteries averages $0.5 \times 10^{-5}\,\mathrm{m}^2$, while errors in the remaining arteries are negligible.

Figure 6. Comparison of pressure and flow-rate simulation results comparison for the ADAN56 network between openBF and (Blanco *et al* 2014). openBF's solution is evaluated at the vessel midpoints.

Despite the overall high similarity in multiple cases, in some patients and in some arteries openBF's area waveforms differ in value from the reference database. This discrepancy can be ascribed to the absence of arterial tapering in openBF's formulation: we assigned a constant radius to all the vessels, which introduces errors when dealing with heavily tapered vessels. Additionally, Charlton *et al* (2019) does not specify the waveform measurement point, which is as an additional source of error when assessing openBF's solution.

A relatively high degree of similarity is observed also for the velocity waveforms. The highest mean distance (3.5×10^{-3} m s^{-1}) is attained in the common iliac artery, with the remaining arteries showing comparable values of normalised distance, between 5×10^{-3} and 3×10^{-3} m s^{-1}.

In terms of pressure, all arteries show similar values of shape similarity with the reference solution, with average DTW error 0.35 mmHg. As with the case of area, openBF's pressure solution in severely tapered arteries differs from Charlton's database in magnitude. We attribute this behaviour to the absence of tapering in openBF, which causes smaller degree of wave reflection.
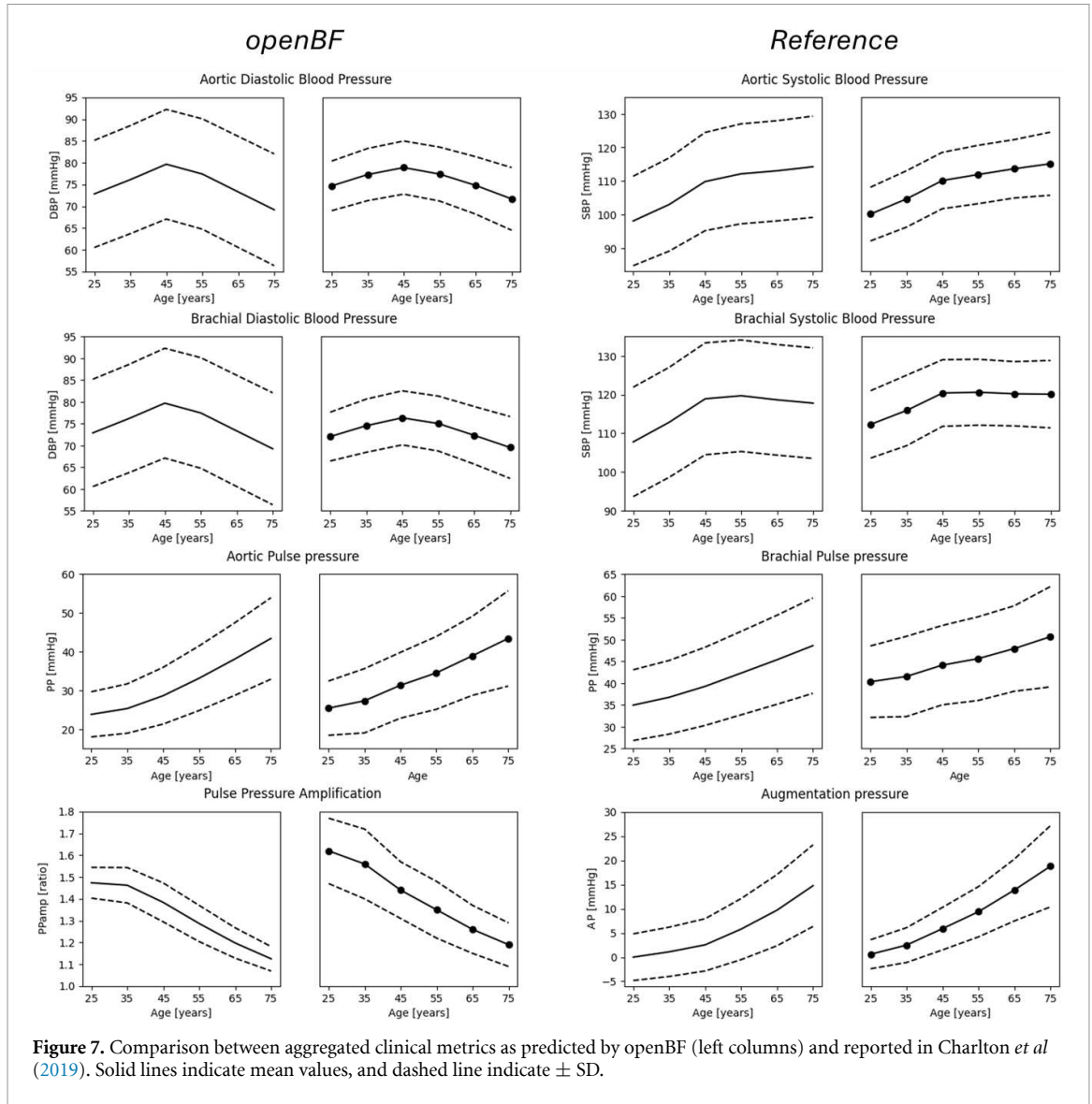
Figure 7. Comparison between aggregated clinical metrics as predicted by openBF (left columns) and reported in Charlton *et al* (2019). Solid lines indicate mean values, and dashed line indicate ± SD.

4.4. Simulation optimisation

Aside from ensuring numerical precision and results correctness, openBF has been optimised to minimise simulation runtime. In figure 9 we report the computational time required for simulating a single cardiac cycle for different solvers (Wéber *et al* 2023) and openBF for elastic and visco-elastic solutions. In openBF case, a scaling study was performed to show the non-linear relationship between computational time and arterial network size. This is particularly relevant as the network grows and smaller arteries are taken into consideration, and is a consequence of how the Courant–Frederich–Levy condition is used to compute the simulation time step:

$$\Delta t \leqslant C_{\mathrm{CFL}} \frac{\Delta x}{c_{\max}}, \tag{8}$$

where C_{CFL} is the Courant–Frederich–Levy number whose value is typically chosen to be 0.9 but can also be set by the user ahead of the simulation. The mesh size Δx is usually taken equal to 1 mm and $c_{\max}$ is the maximum wave speed within the whole network, a quantity inversely proportional to the arteries radii.

openBF runtime increases as the size of the network grows as smaller and stiffer arteries are introduced. Moreover, the visco-elastic solver is consistently slower than the elastic one as an additional numerical step is required.
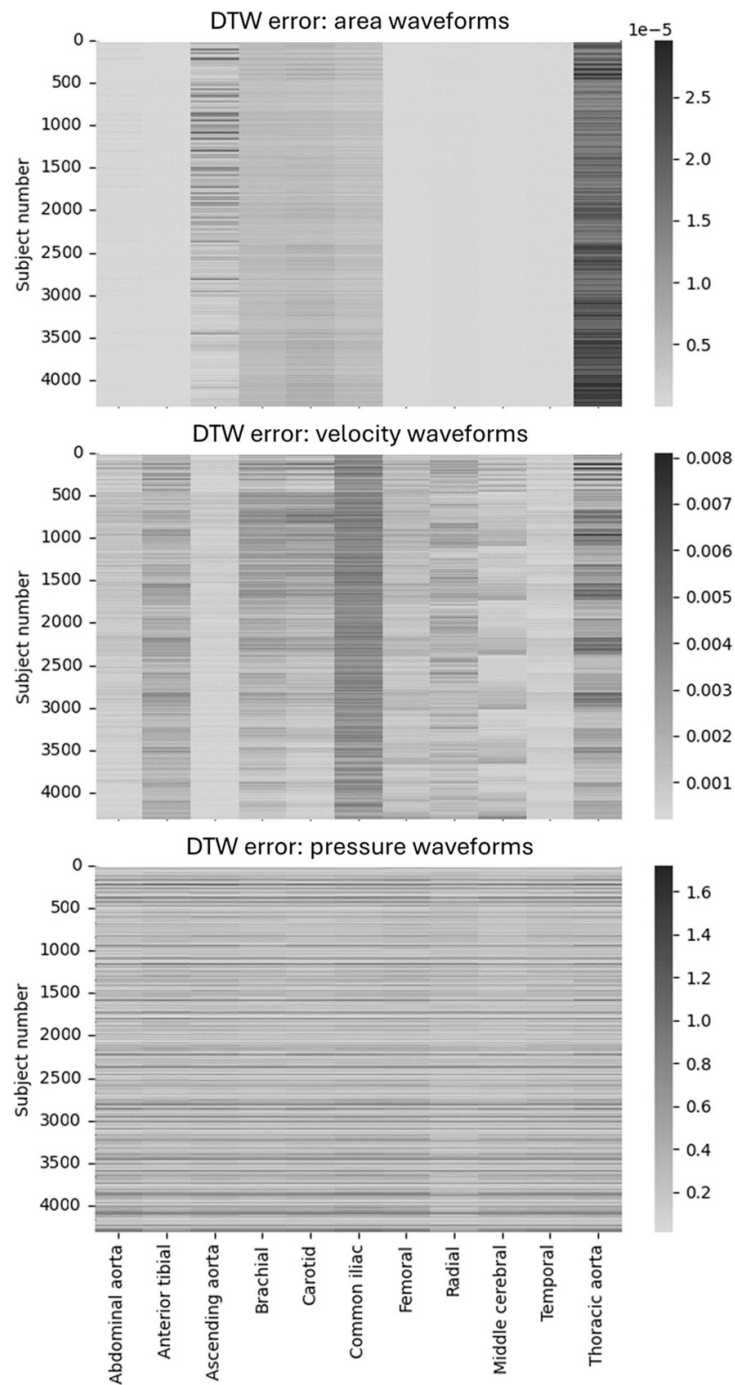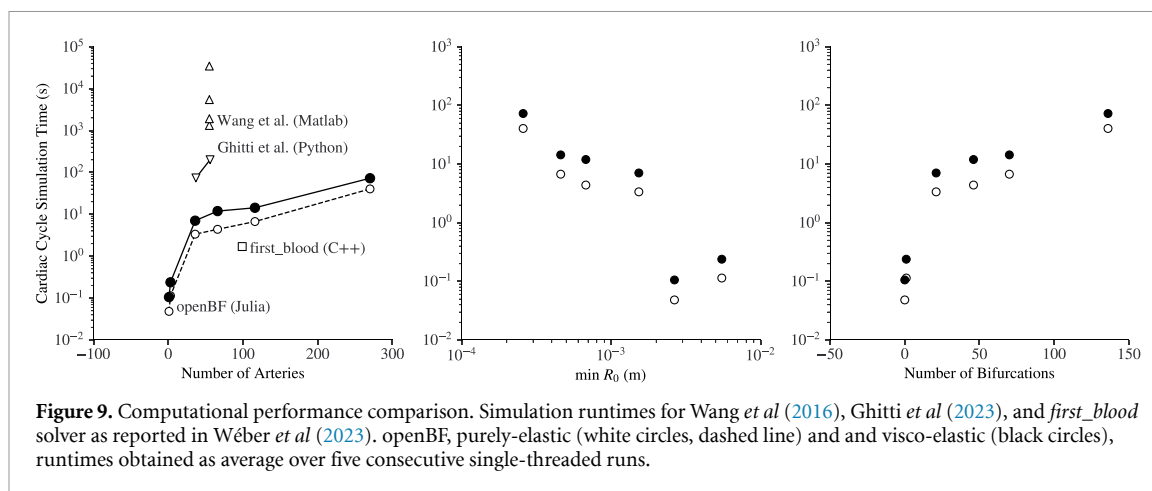
Figure 8. DTW error heatmap between openBF and results from Charlton *et al* (2019) on eleven arteries for the area, velocity and pressure waveforms. Darker colours indicate larger errors.

For the reported simulations, openBF is faster than other solvers based on interpreted languages (i.e. Python and Matlab) and within the same order of magnitude of first_blood, a novel efficient C++ solver. The achieved computational optimisation effectively enables large-scale whole-body population studies to be conducted on affordable workstations rather than relying on HPC facilities.

Figure 9. Computational performance comparison. Simulation runtimes for Wang *et al* (2016), Ghitti *et al* (2023), and *first_blood* solver as reported in Wéber *et al* (2023). openBF, purely-elastic (white circles, dashed line) and and visco-elastic (black circles), runtimes obtained as average over five consecutive single-threaded runs.

5. Conclusions

In this study we presented an updated version of openBF, a finite-volume 1D blood flow solver for networks of compliant vessels. The adopted 1D modelling approach allows for flexible simulations of the cardiovascular system, with the capability of retrieving information about pressure waveform and blood velocity at each point of the computational domain. The code and all the test cases are released under Apache-2.0 open-source license and available on GitHub https://github.com/INSIGNEO/openBF for further development and extensions to the cardiovascular simulation community.

We validated openBF against a number of well established 1D and 3D solutions from the literature. Simulated waveforms show excellent agreement with literature results on all the scales, from single vessel level to full body system and population trends and are obtained with a low computational cost.

Modelling assumptions such as the absence of arterial tapering or non-dissipative bifurcations, can introduce discrepancies between openBF and the solution from other software that currently account for such assumptions, or between openBF and experimental measurements. However, in this study we have shown that the errors with respect to other solvers are in the order of few mmHg for arterial pressure, and fractions of m/s for blood velocities, which are below the variability normally encountered in populations (McEniery *et al* 2014). Further assessments of openBF's predictions will be the topic of future studies, where specific questions of interest, context of uses and experimental and computational comparators will be defined (V&V40 2018).

In this study we have shown that openBF is a valid solution for investigating the behaviour of the cardiovascular system, producing results in excellent agreement with well-established software. Its excellent computational performances make it ideal for studying large populations of patients, and its open-source code fosters contributions from the research community.

Data availability statement

The software is open source, and the data for the simulations are derived from the literature and referenced in the manuscript. The data that support the findings of this study are available upon reasonable request from the authors.

ORCID iDs

I Benemerito ⬤ https://orcid.org/0000-0002-4942-7852
A Melis ⬤ https://orcid.org/0000-0002-8261-0421
A Wehenkel ⬤ https://orcid.org/0000-0001-5022-3999
A Marzo ⬤ https://orcid.org/0000-0002-6702-7932

References

Alastruey J, Khir A W, Matthys K S, Segers P, Sherwin S J, Verdonck P R, Parker K H and Peiró J 2011 Pulse wave propagation in a model human arterial network: assessment of 1-D visco-elastic simulations against in vitro measurements *J. Biomech.* **44** 2250–8

Amini M, Zayeri F and Salehi M 2021 Trend analysis of cardiovascular disease mortality, incidence, and mortality-to-incidence ratio: results from global burden of disease study 2017 *BMC Public Health* **21** 1–12

ASME V&V 40 2018 Assessing credibility of computational modeling through verification and validation: application to medical devices (The American Society of Mechanical Engineers) (available at: https://www.asme.org/codes-standards/find-codes-standards/assessing-credibility-of-computational-modeling-through-verification-and-validation-application-to-medical-devices)

Benemerito I, Mustafa A, Wang N, Narata A P, Narracott A and Marzo A 2023 A multiscale computational framework to evaluate flow alterations during mechanical thrombectomy for treatment of ischaemic stroke *Front. Cardiovascular Med.* **10** 1117449

Benemerito I, Narata A P, Narracott A and Marzo A 2022 Determining clinically-viable biomarkers for ischaemic stroke through a mechanistic and machine learning approach *Ann. Biomed. Eng.* **50** 740–50

Bertaglia G, Navas-Montilla A, Valiani A, Monge García M I M, Murillo J and Caleffi V 2020 Computational hemodynamics in arteries with the one-dimensional augmented fluid-structure interaction system: viscoelastic parameters estimation and comparison with in-vivo data *J. Biomech.* **100** 109595

Bezanson J, Edelman A, Karpinski S and Shah V B 2017 Julia: a fresh approach to numerical computing *SIAM Rev.* **59** 65–98

Blanco P J, Bulant C A, Müller L O, Talou G D M, Bezerra C G, Lemos P A and Feijóo R A 2018 Comparison of 1D and 3D models for the estimation of fractional flow reserve *Sci. Rep.* **8** 17275

Blanco P J, Watanabe S M, Passos M A R F, Lemos P A and Feijóo R A 2014 An anatomically detailed arterial network model for one-dimensional computational hemodynamics *IEEE Trans. Biomed. Eng.* **62** 736–53

Boileau E, Nithiarasu P, Blanco P J, Müller L O, Fossan F E, Hellevik L R, Donders W P, Huberts W, Willemet M and Alastruey J 2015 A benchmark study of numerical schemes for one-dimensional arterial blood flow modelling *Int. J. Numer. Methods Biomed. Eng.* **31** e02732

Caddy H T, Kelsey L J, Parker L P, Green D J and Doyle B J 2024 Modelling large scale artery haemodynamics from the heart to the eye in response to simulated microgravity *npj Microgravity* **10** 7

Cantwell C D *et al* 2015 Nektar++: an open-source spectral/hp element framework *Comput. Phys. Commun.* **192** 205–19

Charlton P H, Mariscal Harana J, Vennin S, Li Y, Chowienczyk P and Alastruey J 2019 Modeling arterial pulse waves in healthy aging: a database for in silico evaluation of hemodynamics and pulse wave indexes *Am. J. Physiol. Heart. Circ. Physiol.* **317** H1062–85

Courant R, Friedrichs K and Lewy H 1928 On the partial difference equations of mathematical physics *Math. Ann.* **100** 32–74

Diem A K and Bressloff N W 2017 VaMpy: a Python package to solve 1D blood flow problems *J. Open Res. Softw.* **5** 17

Fernández M, Milisic V and Quarteroni A 2005 Analysis of a geometrical multiscale blood flow model based on the coupling of ODEs and hyperbolic PDEs *Multiscale Model. Simul.* **4** 215–36

Formaggia L, Gerbeau J, Nobile F and Quarteroni A 2001 On the coupling of 3D and 1D Navier–Stokes equations for flow problems in compliant vessels *Comput. Methods Appl. Mech. Eng.* **191** 561–82

Formaggia L, Lamponi D and Quarteroni A 2003 One-dimensional models for blood flow in arteries *J. Eng. Math.* **47** 251–76

Formaggia L, Quarteroni A and Veneziani A 2010 *Cardiovascular Mathematics: Modeling and Simulation of the Circulatory System* vol 1 (Springer)

Ghigo A R 2017 Reduced-order models for blood flow in networks of large arteries *Theses* Université Pierre et Marie Curie (Paris 6) (available at: https://theses.hal.science/tel-01666313)

Ghitti B, Blanco P J, Toro E F and Müller L O 2023 Construction of hybrid 1D-0D networks for efficient and accurate blood flow simulations *Int. J. Numer. Methods Fluids* **95** 262–312

Guala A, Scalseggi M and Ridolfi L 2017 Coronary fluid mechanics in an ageing cardiovascular system *Meccanica* **52** 503–14

Hellevik L R *et al* 2013 STARFiSh: STochastic ARterial Flow Simulations (available at: http://www.ntnu.no/starfish/)

Kashyap V, Gharleghi R, Li D D, McGrath-Cadell L, Graham R M, Ellis C, Webster M and Beier S 2022 Accuracy of vascular tortuosity measures using computational modelling *Sci. Rep.* **12** 865

Lahtinen J, Moura F, Samavaki M, Siltanen S and Pursiainen S 2023 In silico study of the effects of cerebral circulation on source localization using a dynamical anatomical atlas of the human head *J. Neural Eng.* **20** 026005

LeVeque R J 2002 *Finite Volume Methods for Hyperbolic Problems* vol 31 (Cambridge University Press)

McCullough J W S and Coveney P V 2024 Uncertainty quantification of the lattice Boltzmann method focussing on studies of human-scale vascular blood flow *Sci. Rep.* **14** 11317

McEniery C M, Cockcroft J R, Roman M J, Franklin S S and Wilkinson I B 2014 Central blood pressure: current evidence and clinical importance *Eur. Heart J.* **35** 1719–25

Meert W 2020 DTAIDistance *Zenodo*

Melis A 2017 Gaussian process emulators for 1D vascular models *PhD Thesis* University of Sheffield (available at: https://etheses.whiterose.ac.uk/19175/)

Melis A 2018 openbf: Julia software for 1D blood flow modelling (available at: https://figshare.com/articles/openBF_Julia_software_for_1D_blood_flow_modelling/7166183/1)

Melis A, Moura F, Larrabide I, Janot K, Clayton R, Narata A and Marzo A 2019 Improved biomechanical metrics of cerebral vasospasm identified via sensitivity analysis of a 1D cerebral circulation model *J. Biomech.* **90** 24–32

Milišic V and Quarteroni A 2004 Analysis of lumped parameter models for blood flow simulations and their relation with 1D models *ESAIM: Math. Modelling Numer. Anal.* **38** 613–32

Moura F S, Beraldo R G, Ferreira L A and Siltanen S 2021 Anatomical atlas of the upper part of the human head for electroencephalography and bioimpedance applications *Physiol. Meas.* **42** 105015

Müller L and Toro E 2014 A global multiscale mathematical model for the human circulation with emphasis on the venous system *Int. J. Numer. Methods Biomed. Eng.* **30** 681–725

Müller M 2007 *Information Retrieval for Music and Motion* (Springer) pp 69–84

Mustafa A 2021 An efficient computational approach to guide intervention in treatment of stroke *PhD Thesis* University of Sheffield

Pagoulatou S, Stergiopulos N and Bjornstad P 2017 Evolution of aortic pressure during normal ageing: a model-based study *PLoS One* **12** e0182173

Peiró J and Veneziani A 2009 *In Cardiovascular Mathematics* (Springer) pp 347–94

Reymond P, Merenda F, Perren F, Rüfenacht D and Stergiopulos N 2009 Validation of a one-dimensional model of the systemic arterial tree *Am. J. Physiol. Heart. Circul. Physiol.* **297** H208–22

Seyed Vahedein Y and Liberson A S 2019 Cardiofan: open source platform for noninvasive assessment of pulse transit time and pulsatile flow in hyperelastic vascular networks *Biomech. Model. Mechanobiol.* **18** 1529–48

Sherwin S, Formaggia L, Peiró J and Franke V 2003 Computational modelling of 1D blood flow with variable mechanical properties and its application to the simulation of wave propagation in the human arterial system *Int. J. Numer. Methods Fluids* **43** 673–700

Townsend N, Kazakiewicz D, Lucy Wright F, Timmis A, Huculeci R, Torbica A, Gale C P, Achenbach S, Weidinger F and Vardas P 2022 Epidemiology of cardiovascular disease in Europe *Nat. Rev. Cardiol.* **19** 133–43

Updegrove A, Wilson N M, Merkow J, Lan H, Marsden A L and Shadden S C 2017 SimVascular: an open source pipeline for cardiovascular simulation *Ann. Biomed. Eng.* **45** 525–41

van Leer B 1979 Towards the ultimate conservative difference scheme. V. A second-order sequel to Godunov's method *J. Comput. Phys.* **32** 101–36

Vasan R S, Pan S, Xanthakis V, Beiser A, Larson M G, Seshadri S and Mitchell G F 2022 Arterial stiffness and long-term risk of health outcomes: the Framingham Heart Study *Hypertension* **79** 1045–56

Wang N, Benemerito I, Sourbron S P and Marzo A 2024 An in silico modelling approach to predict hemodynamic outcomes in diabetic and hypertensive kidney disease *Ann. Biomed. Eng.* **52** 1–15

Wang X F, Nishi S, Matsukawa M, Ghigo A, Lagrée P Y and Fullana J M 2016 Fluid friction and wall viscosity of the 1D blood flow model *J. Biomech.* **49** 565–71

Wéber R, Gyürki D and Paál G 2023 First blood: an efficient, hybrid one-and zero-dimensional, modular hemodynamic solver *Int. J. Numer. Methods Biomed. Eng.* **39** e3701

Wehenkel A, Behrmann J, Miller A C, Sapiro G, Sener O, Cuturi M and Jacobsen J H 2023 Simulation-based inference for cardiovascular models (arXiv:2307.13918)

Xiao N, Humphrey J D and Figueroa C A 2013 Multi-scale computational model of three-dimensional hemodynamics within a deformable full-body arterial network *J. Comput. Phys.* **244** 22–40